Nuclear Engineering and Technology 56 (2024) 3796–3803

Contents lists available at ScienceDirect

Nuclear Engineering and Technology

journal homepage: www.elsevier.com/locate/net

Original Article

Studies on structural, optical, thermal and low energy shielding for gamma rays for the ZSBP glasses

Abeer S. Altowyan [a], M.I. Sayyed [b,c,**], Ashok Kumar [d,e,*]

[a] Department of Physics, College of Science, Princess Nourah bint Abdulrahman University, P.O. Box 84428, Riyadh, 11671, Saudi Arabia
[b] Department of Physics, Faculty of Science, Isra University, Amman, Jordan
[c] Renewable Energy and Environmental Technology Center, University of Tabuk, Tabuk, 47913, Saudi Arabia
[d] University College, Benra, Dhuri, 148024, Punjab, India
[e] Department of Physics, Punjabi University, Patiala, 147002, Punjab, India

ARTICLE INFO

Keywords:
Glass
UV–Vis
Raman
DTA
DSC
Gamma ray shielding

ABSTRACT

By employing the melt-quenching technique, the ZnO–SrO–B_2O_3–PbO (ZSBP) glasses have been successfully fabricated. The derivative of Absorption Spectra Fitting (DASF) method was used to study the energy band gap (E_g) of the glasses which decreases from 3.57 eV to 3.39 eV. The structural properties have been studied using the Raman spectroscopy. The glass transition temperature (T_g) decreases with increase in concentration of the lead oxide. The current study examines the radiation shielding properties at 30.80–444 keV. The addition of PbO to the glasses resulted in a proportionate increase in the mass attenuation coefficient (MAC), suggesting a diminishing tendency in radiation transmission. At 30.80 keV, the MAC values are extremely high and range from 18.06 to 21.11 cm^2/g. As density rises, the half value layer (HVL) decreases. In addition, the average HVL ($\overline{HVL}$) decreases. The glass thickness required to reduce the radiation intensity to 90 %, 50 %, 25 %, and 10 % of its initial value is investigated at an energy of 35.80 keV. The T90 %, T50 %, T25 %, and T10 % values are 0.0020, 0.0132, 0.0264, and 0.0439 cm, respectively. The results suggest that a greater thickness of the radiation barrier is necessary to attain the necessary degree of attenuation.

1. Introduction

Radiation protection glasses are very important for keeping people safe from the harmful effects of radiation, which can be very bad for both people and the environment. Radiation technologies, like X-rays and radiation treatment, can save lives in medicine and other fields, like food storage and energy production. However, being exposed to radiation for a long time is very dangerous. To lower these risks, it is important to make radiation protection materials that work [1–7].

As a result of being clear, flexible, and inexpensive, glasses are one of the most common objects used to block radiation [8–12]. Borate glasses, which are mostly made up of boron oxide, are becoming more and more popular as radiation protection materials because they are resistant to chemicals and heat, easy to make, and cheap. Borate glasses have benefits like being safe for the environment, being clear, and being able to be used for real-time tracking. More and more people are interested in studying how well high-density metal oxide glasses, especially borate-based glasses [13–16], block radiation in recent years. By changing the ingredients in borate glasses, you can make them better at blocking different kinds of radiation, like X-rays and fast neutrons. To make them work better with certain types of radiation and photon energies, however, the glass makeup can be changed by adding more metal oxides like ZnO, SrO and PbO [17–21]. Not only do these changes make the glasses' structure and physicochemical qualities better, but they also make them better at blocking radiation. As the addition of the higher atomic number elements improves density. It results in increasing the probability of interactions, thereby providing more effective protection against harmful radiation exposure in various applications, including nuclear power plants, medical facilities, and space exploration.

To make new glasses with specific qualities, it is also important to study the optical, thermal, and structural aspects of different glass systems. Not only do these qualities affect how well radiation protection works, but they also help the development of photonic devices and other uses. Even though it is learnt a lot about how glasses work, there are still

* Corresponding author.
** Corresponding author.
E-mail addresses: dr.mabualssayed@gmail.com (M.I. Sayyed), ajindal9999@gmail.com (A. Kumar).

https://doi.org/10.1016/j.net.2024.04.028
Received 13 March 2024; Received in revised form 5 April 2024; Accepted 18 April 2024
Available online 20 April 2024

some things that need to be looked into further. So, the main goal of this study is to look into the optical, physical, radiation-blocking, and structural features of glasses made of borates, especially those that contain ZnO, SrO, PbO, and B_2O_3. The E_g of the glasses decreases from 3.57 eV to 3.39 eV and T_g decreases with increase in concentration of the PbO. As density rises, the HVL and $\overline{HVL}$ decreases as a result of the PbO addition to the glasses. By looking at these qualities in more depth, one can learn more about radiation protection materials and come up with better ways to protect people from the harmful effects of radiation exposure.

2. Materials and methods

2.1. Glass preparation

By employing the melt-quenching technique, the ZSBP glasses have been successfully fabricated. Using a high-precision electronic scale with a resolution of 0.001 g, the precise quantities of oxides of analytical reagent grade has been measured for the fabrication of the samples. The amount of the oxides has been taken in accordance with the molar composition criteria outlined in Table 1. ZSBP1, ZSBP2, ZSBP3, and ZSBP4 are the names given to the glasses. It is necessary to utilise an agate mortar in order to create the homogeneous powder. The resulting powdery mixture has been placed inside of a muffle furnace after being deposited onto an alumina crucible. For the purpose of ensuring that the melt was consistent throughout, the temperature was raised to 950°C and maintained for a period of 2 h while stirring at regular intervals. After that, the liquid combination has been transferred to a graphite mould and then placed in a separate furnace that was maintained at 300°C for the purpose of annealing. Following that, the material was allowed to remain undisturbed for a period of 24 h. Thereafter, the specimens have been collected for the purpose of conducting future analytical examinations. The densities of the samples are measured using the Archimedes' principle.

2.2. Ultraviolet–visible (UV–vis) spectroscopy

The UV–Vis spectra have been recorded using the PerkinElmer Lambda 19 UV–Vis–NIR spectrophotometer, which covers a wavelength range of 180–800 nm. The Tauc plot approach, using UV–Vis absorption data, was employed to determine the E_g and assess further optical properties.

2.3. Raman spectroscopy

The Raman spectra were obtained using the STR500Airix Confocal Raman Spectrometer, which has exceptional resolution. The instrument utilises a 532 nm laser.

2.4. Measurement of thermal properties

The STA 6000, a state-of-the-art thermal analysis device manufactured by PerkinElmer, was utilised to analyse and determine the thermal characteristics. The apparatus utilised dual-furnace technology to perform simultaneous differential scanning calorimetry (DSC) and thermogravimetric analysis (TGA), allowing for the examination of thermal stability and decomposition.

Table 1
Composition and other parameters of the ZSBP glasses.

Glass code	Moles of oxides present				ρ (g/cm^3)	E_g (eV)	T_g (°C)
	ZnO	SrO	B_2O_3	PbO			
ZSBP1	0.10	0.10	0.45	0.35	4.292	3.57	416
ZSBP2	0.10	0.10	0.40	0.40	4.515	3.48	392
ZSBP3	0.10	0.10	0.35	0.45	4.731	3.46	374
ZSBP4	0.10	0.10	0.30	0.50	4.922	3.39	369

2.5. Gamma ray shielding

The goal of this work is to understand radiation shielding properties at low energies between 30.80 and 444 keV. The certain radiation attenuation parameters have been assessed using the chemical composition of these glasses as input data in the Phy-X program [22]. Eq. (1) presents a method of evaluating the linear attenuation coefficient (LAC) using Lambert-Beer's law equation as:

$$I = I_0 e^{-LAC.\ t} \tag{1}$$

The mass attenuation coefficient (MAC), another density-independent data, is related to the LAC.

For any glass sample, the MAC via the mixture rule can be written as:

$$MAC = \sum_i w_i (MAC)_i \tag{2}$$

The HVL, tenth value layer (TVL) and the mean free path (MFP) need to be assessed in order to determine the sample thickness needed for the radiation beam to be attenuated to a specific level. It is possible to alter the HVL of some glasses by adjusting their density and chemical makeup. The HVL can be expressed mathematically as [23–26]:

$$HVL = \frac{0.693}{LAC} \tag{3}$$

Using the following formula, the TVL for the current glasses can be determined as:

$$TVL = \frac{2.3}{LAC} \tag{4}$$

Researchers and investigators may develop space-efficient shields in situations when radiation doses need to be reduced to significantly lower levels by looking at the two characteristics mentioned above for specific glasses.

A glass sample's MFP is inversely equal to its LAC, specifically equal to as:

$$MFP = \frac{1}{LAC} \tag{5}$$

Also, the next equation may be applied to estimate the sample's effective atomic number (Z_{eff}) as:

$$Z_{eff} = \frac{\sum_i f_i A_i \left(\frac{\mu}{\rho}\right)_i}{\sum_j f_j \frac{A_j}{Z_j} \left(\frac{\mu}{\rho}\right)_j} \tag{6}$$

3. Results and discussion

3.1. Optical properties

The DASF method is based on the expression given as [27–29]:

$$\frac{d\left\{ln\left[\frac{A(\lambda)}{\lambda}\right]\right\}}{d\left\{\frac{1}{\lambda}\right\}} = \frac{m}{\left(\frac{1}{\lambda} - \frac{1}{\lambda_g}\right)} \tag{7}$$

Where λ_g is the wavelength at which the derivative plot exhibits a discontinuity, m is a constant, and A(λ) is the absorption intensity at a particular wavelength λ.

In this study, the derivative of the natural logarithm of the rounded ratio of A(λ) to λ with respect to the reciprocal of wavelength, denoted as $\frac{d\left\{ln\left[\frac{A(\lambda)}{\lambda}\right]\right\}}{d\left\{\frac{1}{\lambda}\right\}}$, is illustrated against 1/λ, as shown in Fig. 1. In particular, a plot discontinuity indicates a single location where the derivative changes abruptly. At this crucial point, the material passes through an

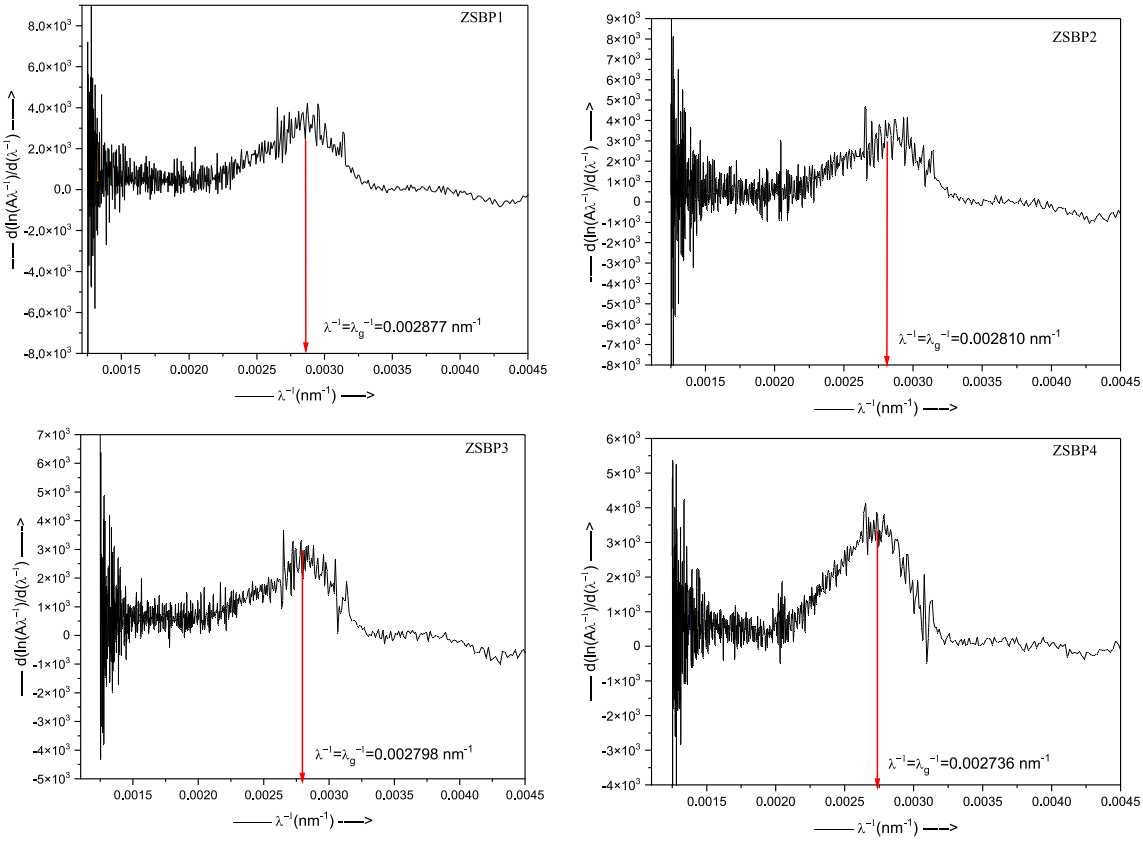

Fig. 1. The $\frac{d\{ln\left|\frac{A(\lambda)}{\lambda}\right|\}}{d\{\frac{1}{\lambda}\}}$ vs. 1/λ for measuring the discontinuity.

electronic transition, and the wavelength at which it does so is represented by $\frac{1}{\lambda} = \frac{1}{\lambda_g}$. The equation $E_g = \frac{1239.82}{\lambda_g} eV$ is then used to get the E_g from the appropriate wavelength, λ_g, linked to this discontinuity.

The discontinuities aligned with $\frac{1}{\lambda} = \frac{1}{\lambda_g}$ are measured as 0.002877 nm^{-1}, 0.002810 nm^{-1}, 0.002798 nm^{-1} and 0.002736 nm^{-1} for the ZSBP1, ZSBP2, ZSBP3, and ZSBP4 samples, respectively, in Fig. 1. The E_g values for the ZSBP1, ZSBP2, ZSBP3, and ZSBP4 samples are 3.57 eV, 3.48 eV, 3.46 eV, and 3.39 eV, respectively, according to the above equation (Table 1). Based on these results, it seems that electrical transitions inside the glass structure need less energy. The structural changes caused by the weakening of metal-oxygen bonds, which increase the quantity of non-bridging oxygens (NBOs), are responsible for this decrease [30]. As a result, PbO's presence makes it easier for the glass matrix to generate NBOs, which in turn adds additional energy levels to the band structure and reduces the energy needed to bridge the band gap.

3.2. Structural properties

The Raman spectrum is depicted in Fig. 2. The nine peaks are observed in the spectra about~145 cm^{-1}, ~310 cm^{-1}, ~590 cm^{-1}, ~640 cm^{-1}, ~725 cm^{-1}, ~925 cm^{-1}, ~1005 cm^{-1}, ~1225 cm^{-1} and ~1300 cm^{-1} respectively.

The Raman spectra show the first peak about~145 cm^{-1}, which can be attributed to the symmetric stretching vibration of Pb–O bonds [31–33]. The presence of PbO_4 units is supported by the simultaneous development of a wide spectral feature about ~310 cm^{-1}. Nevertheless, the possibility of minor contributions from soft modes associated with borate in this frequency range cannot be entirely ruled out [31–35]. The Raman peaks at about ~1225 cm^{-1} appears to exhibit a fast growth with

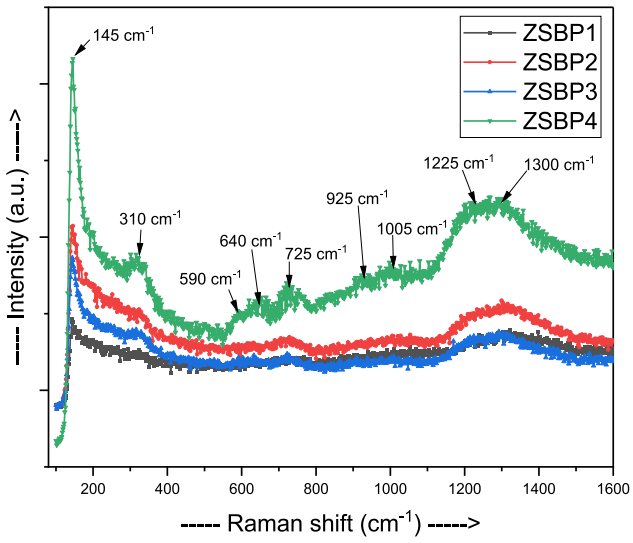

Fig. 2. The Raman plot for the ZSBP glasses.

increasing lead concentrations. This phenomenon is indicative of the stretching of B-Ō bonds in metaborate triangles ($B\emptyset_2\bar{O}$), mostly resulting in the formation of chain-like structures [36]. The evidence for this is supported by the simultaneous rise in intensity of two bands about ~640 cm^{-1} and ~725 cm^{-1}, which are associated with the deformation modes of metaborate chains [36–38]. The peak at around ~590 cm^{-1}

indicates the disintegration of diborate groups and the creation of "loose" $B\emptyset_4^-$ units, namely borate tetrahedra that link various structural segments. The asymmetric stretching motion of anions in B–O–Pb, B–O–Sr, and B–O–Zn bridges may account for the peak around ~930 cm^{-1}. The Raman signal about ~1005 cm^{-1} indicates the B–O stretching vibration of BO_4 in BO_3- units [39]. The B–O^- stretching activity is demonstrated by the metaborate triangles coupled to the tetrahedral BO_4^- groups by π-electronic interactions, which are responsible for the peak about ~1300 cm^{-1}. Hence, the glassy network's BO_4^- units may be indirectly probed by observing the spectral shape of the B–O^- stretching. It is well knowledge that pentaborate glass networks often include borate configurations that include tetrahedral BO_4^- and triangular metaborate units, where the three- and four-coordinated units undergo isomerisation [40,41].

3.3. Thermal properties

TGA studies are plotted in Fig. 3. The glasses with least concentration of lead oxide lose 3 % of its weight when the temperature of the samples is increased up to 800°C. The glasses with higher concentration of lead oxide are losing even less than 1 % of its weight with rise in temperature. So one can conclude that increasing consideration of lead oxide in the glasses contributes towards thermal stability of the glasses [42]. The DSC plots are shown in Fig. 4. The T_g has been marked on the curves. The T_g decreases with PbO content (Table 1). The higher size of lead oxide results in the opening the network due to this network becomes less stable and more disordered due to this of the T_g of the glasses decreases [43,44].

3.4. Gamma ray shielding properties

The MAC for the selectedZSBP1, ZSBP2, ZSBP3 and ZSBP4 glasses was determined using the Phy-X software at low energy range of 30.82–444 keV. This energy range is selected since these energies are typical emissions from Ba-133 and Eu-152, both of which are known for their important utilizations in different technological applications. The MAC for the ZSBP-X glasses is represented in Fig. 5. The maximum MAC values were found for ZSBP4 in the low energy range under study. The MAC varied from 21.106 to 0.162 cm^2/g at 30.82–444 keV. The photoelectric effect (PE), which is the main mode of interaction with such low levels of energy radiation, can account for the observed phenomenon of elevated MAC for these glasses between 30.82 and 53.16 keV. The cross-section of this mechanism rises dramatically with the atomic number of the sample. These glasses have a higher PE cross-section due

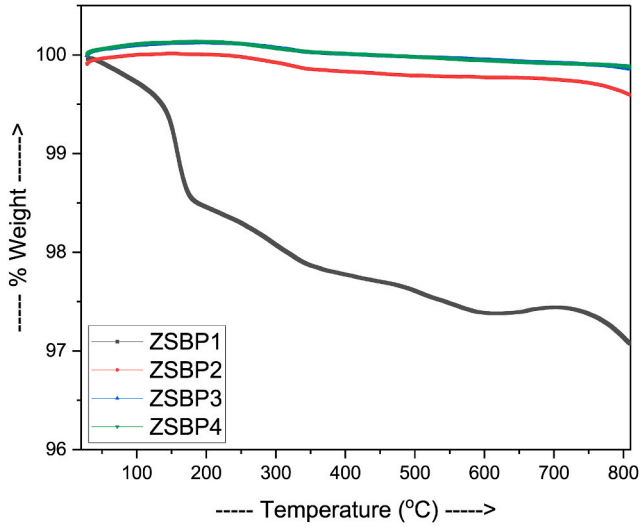

Fig. 3. The TGA plot for the ZSBP glasses.

Fig. 4. The DSC plot for the ZSBP glasses.

Fig. 5. The MAC ZSBP glasses at low energy region of 30.80–444 keV.

to the presence of Zn, Sr, and Pb, which results in high MAC values between 30.82 and 53.16 keV. A sharp decline is observed in the MAC with increasing energy, with a single exception at 121.8 keV. PE becomes less significant as energy increases, but Compton scattering (CS) becomes more prevalent. The CS cross-section is weakly reliant on the atomic number of the shielding medium. As a result, at high energies, the MAC for each glass converges. Notably, at 121.8 keV, the MAC for the four glasses increases, diverging from the usual pattern of MAC decreasing with energy. The K-absorption edge of Pb is responsible for the observed increase in MAC at 121.8 keV. Doping with lead oxide, on the other hand, was found to result in an increase in the MAC. This shows that there is a correlation between the MAC and their elemental composition. The amount of B_2O_3 decreases from glass ZSBP1 to ZSBP4, while PbO increases at the same time. The MAC shows this compositional shift clearly, with ZSBP4 having the largest MAC and ZSBP1 having the least amount of MAC. This finding highlights the impact of elemental replacement on the MAC of the glasses by indicating a strong link between the inclusion of the denser component PbO and the increase in MAC.

The LAC of the produced samples at 35.4 keV is displayed to better understand how adding PbO affected the glasses' ability to shield photons (Fig. 6). The produced glasses' LAC values are strongly influenced

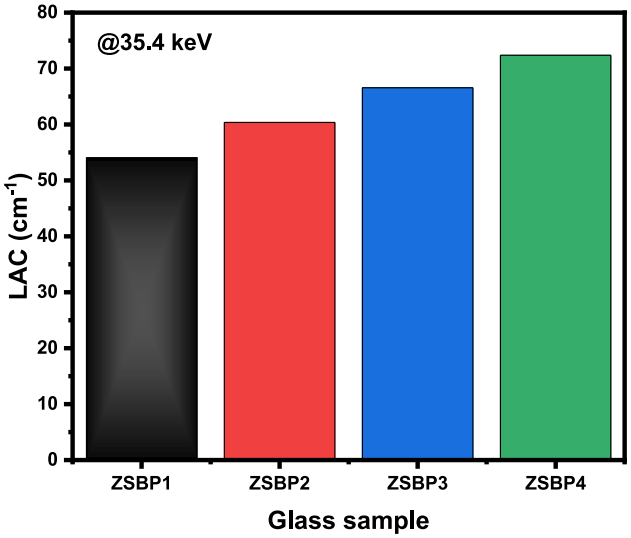

Fig. 6. The LAC for the ZSBP glasses at 35.4 keV.

by the reinforcing compounds, as Fig. 6 illustrates. When PbO is substituted for B_2O_3, the LAC at 35.34 keV rises from 53.99 to 72.37 cm^{-1}. The density of the medium affects the LAC. Compared to glasses containing 35, 40, and 45 mol% PbO, the glass containing 50 mol% PbO has a greater LAC. The data for 35.4 keV gamma rays is presented, although this conclusion is likewise consistent for the other energies examined. Thus, a high PbO content has a high LAC and performs well attenuation.

The HVL is displayed in Fig. 7. According to the data in Fig. 7, the HVL for all prepared glasses is trending increasing as energy levels rise. This HVL behavior can be explained by the inverse relationship between the HVL and LAC values. A more thick glass is needed to reduce the intensity of photons. For instance, for ZSBP1, the HVL is 0.009 cm at 30.82 keV, increases to 0.012 cm at 35 keV, to 0.017 cm at 39.50 keV, and to 0.156 cm at 160.6 keV. Additionally, at 121.80 keV, a sharp drop is observed in the HVL for all glasses; for ZSBP1, this energy corresponds to an HVL of 0.080 cm, whereas for ZSBP4, it is 0.059 cm. These glasses have high LAC values at 121.80 keV, which helps to explain the abrupt reduction in the HVL at this energy level. Furthermore, the HVL of these glasses varies with PbO content. Since adding PbO obviously lowers the HVL, the produced glass with the highest PbO content, ZSBP4, had the lowest HVL of all the glasses.

For the energy ranges of 30.82–81 keV and 160.6–444 keV, the average HVL ($\overline{HVL}$) is computed in two different scenarios. As previously indicated, the HVL exhibits an opposing trend at energy of 121.8 keV. The $\overline{HVL}$ is plottedfor the two energy ranges in Figs. 8 and 9 respectively. An analysis of $\overline{HVL}$ demonstrates the important trend in the attenuation characteristics of the glasses and their capacity to prevent radiation penetration at various energies. The HVL drops from the ZSBP1 sample to the ZSBP4 sample in both energy regions. For example, the HVL decreases from 0.028 to 0.021 cm in Fig. 8 and from 0.637 to 0.499 cm in Fig. 9. This suggests that ZSBP4 is the best shielding sample between 30.82–81 keV and 160.6–444 keV, with ZSBP3, ZSBP2, and ZSBP1 following in that order of effectiveness. Out all the glasses described, ZSBP1 is the least effective shield since it has the biggest $\overline{HVL}$ for both the energy ranges shown in Figs. 8 and 9. Furthermore, it was obvious that the $\overline{HVL}$ values obtained for the energy range of 160.6–444 keV are greater than those obtained for the energy range of 30.82–81 keV.For example, the $\overline{HVL}$ for ZSBP1 in Fig. 8 is 0.028 cm, while it is 0.637 cm for this glass for the energy range of 160.6–444 keV. This suggests that, in comparison to radiation with extremely low energy of 30.82–81 keV, photons with an energy of 160.6–444 keV penetrate the prepared specimens a greater distance.

To find out how successfully these glasses attenuate photons, a variety of parameters were derived that showed the drop in incoming photon intensity as they pass through a specific thickness of glass. These kinds of components establish the necessary thickness for a decrease in intensity. In order to construct shielding materials and understand photon penetration via different materials, these properties need to be calculated. Fig. 10 shows the ZSBP1 thickness required to reduce the level of radiation with energy of 35.8 keV–90 %, 50 %, 25 %, and 10 % of its initial value. The following symbols are used to represent these parameters: T90 %, T50 %, T25 %, and T10 %, in that order. Since X90 % indicates a very slight attenuation of the photons, the attenuation was only 0.0020 cm. Consequently, a very thin layer of ZSBP1 is to be used if only a small reduction in photon intensity with energy of 35.80 keV is needed. The $T_{50\ \%}$ is 0.0132 cm, whereas the $T_{25\ \%}$ and $T_{10\ \%}$ are 0.0264 and 0.0439 cm respectively. Consequently, the results show that if there are higher demands on radiation reduction, the sample must be thicker at the same energy.

Additionally, the Z_{eff} of the designed glasses is calculated at low energy range (Fig. 11). Between 30.80 and 444 keV, the Z_{eff} clearly falls with increasing energy, but at 121.80 keV, it exhibits an increasing

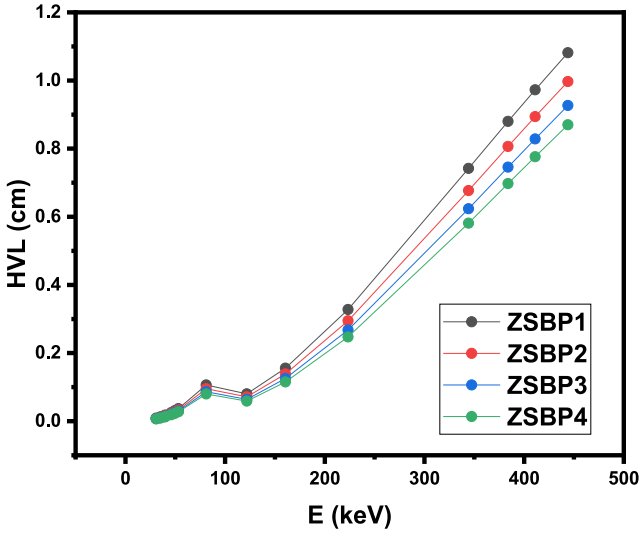

Fig. 7. The HVL for the ZSBP glasses at low energy range of 30.80–444 keV.

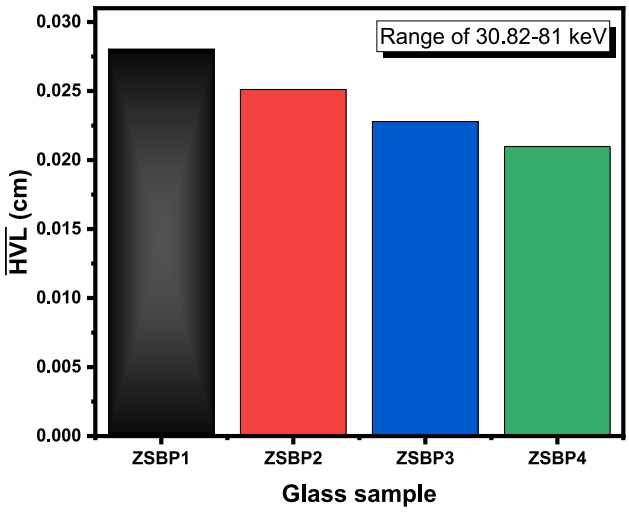

Fig. 8. The $\overline{HVL}$ in the energy range of 30.82–81 keV.

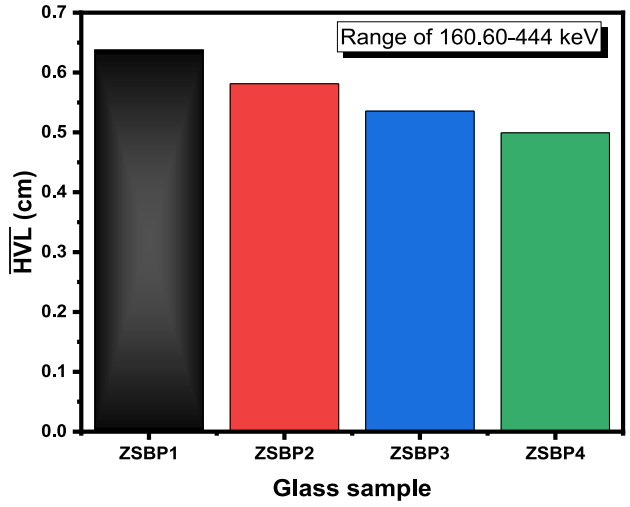

Fig. 9. The $\overline{HVL}$ in the energy range of 160.6–444 keV.

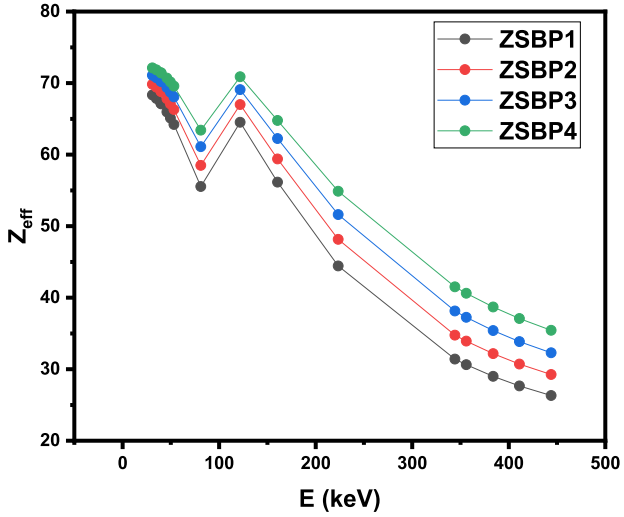

Fig. 11. The Z_{eff} for the ZSBP glasses at low energy region of 30.80–444 keV.

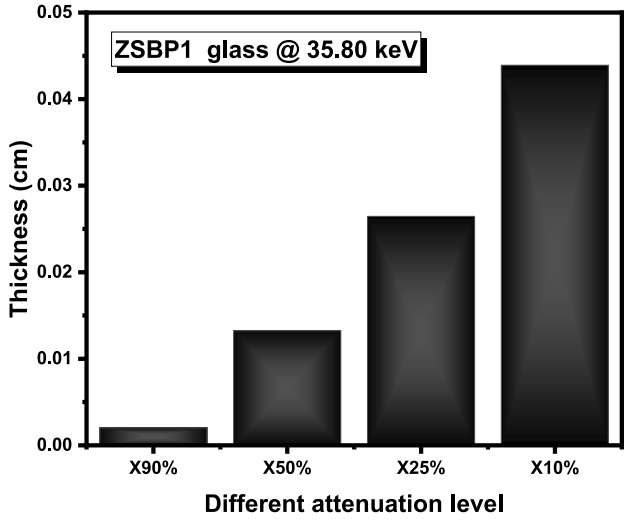

Fig. 10. The thickness of the ZSBP1 sample required to attenuate photons at 35.80 keV to certain specified levels.

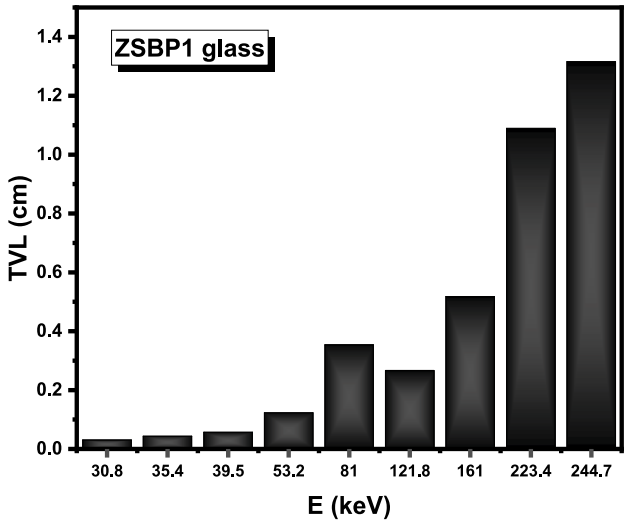

Fig. 12. The TVL for ZSBP1 at some selected energies.

tendency.

As the atomic number of the shield components has a significant impact on PE cross-section, the Z_{eff} is very high at 30.80 keV and varies between 68.33 and 72.13. The K absorption edge of Pb can account for the abrupt increase in the Z_{eff} at 121.80 keV. Furthermore, the findings showed that the Z_{eff} is altered by the glasses' chemical composition. It is crucial to remember that as the B_2O_3 content falls, the PbO concentration raises from ZSBP1 to ZSBP4. The highest Z_{eff} results for ZSBP4can therefore be explained by the glass exhibiting a higher Z_{eff} due to its higher PbO content.

In Fig. 12, the TVL for ZSBP1 is displayed at various energies. The findings showed that the TVL is only 30.80 keV (0.030 cm), which indicates that a thin glass is required for attenuating very low energy photons. The TVL rises to 0.043 cm as the energy grows to 35.40 keV and to 0.353 cm as the energy increases to 81 keV. With the exception of 121.80 keV, the TVL generally rises as energy does. This implies that ZSBP1 is more effective when it comes to photons with lower energy.

4. Conclusion

By employing the melt-quenching technique, the ZSBP glasses have been successfully fabricated. The E_g decreases from 3.57 eV to 3.39 eV with addition of PbO. The various stretching and bending vibrations present in the ZSBP glasses have been studied using the Raman spectroscopy. The T_g decreases with increase in PbO content. Moreover, this study investigated the radiation shielding capabilities of the glasses at low energies between 30.80 and 444.44 keV. The MAC increased proportionately when PbO was added to the glasses, indicating a tendency toward decreasing radiation transmission. The LAC at 35.4 keV for the prepared glasses increased from 53.99 to 72.37 cm^{-1} when the PbO content increases between 35 and 50 mol%. Additionally, the addition of PbO to the glasses results in a decrease in the average HVL ($\overline{HVL}$). At energy of 35.80 keV, the thickness of glass needed to lower the radiation intensity to 90 %, 50 %, 25 %, and 10 % of its initial value. T90 %, T50 %, T25 %, and T10 % are represented by the values 0.0020, 0.0132, 0.0264, and 0.0439 cm, in that order. The findings imply that in order to achieve the required level of attenuation, a thicker radiation barrier is required.

Data availability

The datasets generated during and/or analysed during the current study are available from the corresponding author on reasonable request.

Code availability

Not applicable.

Ethics approval

Not applicable.

Consent to participate

Not applicable.

Consent for publication

Not applicable.

Competing interests

Not applicable.

Funding

The authors express their gratitude to the Princess Nourah bint Abdulrahman University Researchers Supporting Project number (PNURSP2024R16), Princess Nourah bint Abdulrahman University, Riyadh, Saudi Arabia.

CRediT authorship contribution statement

Abeer S. Altowyan: Funding acquisition, Writing – review & editing. **M.I. Sayyed:** Conceptualization, Writing – original draft, Writing – review & editing. **Ashok Kumar:** Conceptualization, Data curation, Investigation, Writing – original draft, Writing – review & editing.

Declaration of competing interest

The authors declare that they have no known competing financial interests or personal relationships that could have appeared to influence the work reported in this paper.

Acknowledgment

The authors express their gratitude to the Princess Nourah bint Abdulrahman University Researchers Supporting Project number (PNURSP2024R16), Princess Nourah bint Abdulrahman University, Riyadh, Saudi Arabia.

References

[1] Nurul Ihsani Rifqah, Lobo Gareso Paulus, Dahlang Tahir, An overview of gamma radiation shielding: enhancements through polymer-lead (Pb) composite materials, Radiat. Phys. Chem. 218 (2024) 111619.
[2] A. Alshamari, M. Mhareb, N. Alonizan, M.I. Sayyed, N. Dwaikat, I. Alrammah, M. K. Hamad, Q. Drmosh, Gamma-ray-induced changes in the radiation shielding, structural, mechanical, and optical properties of borate, tellurite, and borotellurite glass systems modified with barium and bismuth oxide, Optik 281 (2023) 170829.
[3] A.A. Rotkovich, D.I. Tishkevich, S.A. German, A.A. Bondaruk, E.S. Dashkevich, A. V. Trukhanov, A study of the morphological, structural, and shielding properties of epoxy-W composite materials, Nexus of Future, Materials 1 (2024) 13–19. https://nfmjournal.com/articles/5.
[4] A. Aşkın, M.I. Sayyed, Amandeep Sharma, M. Dal, R. El-Mallawany, M.R. Kaçal, Investigation of the gamma ray shielding parameters of (100-x)[0.5Li_2O–0.1B_2O_3–0.4P_2O_5]-xTeO_2 glasses using Geant4 and FLUKA codes, J. Non-Cryst. Solids 521 (2019) 119489.
[5] M.K. Hamad, Evaluation of photon shielding properties for new refractory tantalum-rich sulfides $Ta_9(XS_3)_2$ alloys: a study with the MCNP-5, Ann. Nucl. Energy 184 (2023) 109687.
[6] Qiuling Chen, K.A. Naseer, K. Marimuthu, P. Suthanthira Kumar, Baoji Miao, K. A. Mahmoud, M.I. Sayyed, Influence of modifier oxide on the structural and radiation shielding features of Sm^{3+}- doped calcium telluro-fluoroborate glass systems, Journal of the Australian Ceramic Society 57 (2021) 275–286.
[7] M.S. Al-Buriahi, M. Rashad, Amani Alalawi, M.I. Sayyed, Effect of Bi_2O_3 on mechanical features and radiation shielding properties of boro-tellurite glass system, Ceram. Int. 46 (2020) 16452–16458.
[8] M.H.A. Mhareb, Y.S.M. Alajerami, M.I. Sayyed, Nidal Dwaikat, Muna Alqahtani, Fatimh Alshahri, Noha Saleh, N. Alonizan, Taher Ghrib, Sarah Ibrahim Al-Dhafar, Radiation shielding, structural, physical, and optical properties for a series of borosilicate glass, J. Non-Cryst. Solids 550 (2020) 120360.
[9] Nuri Yorulmaz, Mehmet Murat Yasar, Abuzer Acikgoz, Yusuf Kavun, Gokhan Demircan, Mirac Kamislioglu, Bulent Aktas, Esmanur Oruc Ulas, Influence of Gd_2O_3 on structural, optical, radiation shielding, and mechanical properties of borate glasses, Opt. Mater. 149 (2024) 115032.
[10] R. Divina, G. Sathiyapriya, K. Marimuthu, A. Askin, M.I. Sayyed, Structural, elastic, optical and γ-ray shielding behavior of Dy^{3+} ions doped heavy metal incorporated borate glasses, J. Non-Cryst. Solids 545 (2020) 120269.
[11] M.A. Imheidat, M.K. Hamad, M.I. Sayyed, Y. Alajerami, N.S. Prabhu, S.D. Kamath, M.H. Flaifel, M.H. Mhareb, Correlation between mechanical, gamma shielding features and tellurium oxide concentrations in molybdenum aluminum strontium borate glass, Optik 272 (2023) 170336.
[12] A. Alshamari, M. Mhareb, N. Alonizan, M.I. Sayyed, N. Dwaikat, I. Alrammah, M.K. Hamad, Q. Drmosh, Gamma-ray-induced changes in the radiation shielding, structural, mechanical, and optical properties of borate, tellurite, and borotellurite glass systems modified with barium and bismuth oxide. Optik 281, 170829. https://doi.org/10.1016/j.ijleo.2023.170829.
[13] M.H.A. Mhareb, Muna Alqahtani, Fatimh Alshahri, Y.S.M. Alajerami, Noha Saleh, N. Alonizan, M.I. Sayyed, M.G.B. Ashiq, Taher Ghrib, Sarah Ibrahim Al-Dhafar, Tasneem Alayed, Mohamed A. Morsyh, The impact of barium oxide on physical, structural, optical, and shielding features of sodium zinc borate glass, J. Non-Cryst. Solids 541 (2020) 120090.
[14] Yusuf Kavun, Hasan Eskalen, Mustafa Kavgacı, Hakan Yaykaşlı, Medeni Bahşi, A novel vanadium pentoxide doped glasses characterization for radiation shielding applications, Appl. Radiat. Isot. 203 (2024) 111086.
[15] M.K. Hamad, M.H. Mhareb, M.I. Sayyed, Y. Alajerami, R. Alsharhan, M. U. Khandaker, Novel efficient alloys for ionizing radiation shielding applications: a theoretical investigation, Radiat. Phys. Chem. 200 (2022) 110181.
[16] M.H. Mhareb, M.I. Sayyed, S. Hashim, M. Alshammari, S. Alhugail, H. Aldoukhi, M. K. Hamad, Y. Alajerami, M.U. Khandaker, Radiation shielding features for a new glass system based on tellurite oxide, Radiat. Phys. Chem. 200 (2022) 110094.
[17] Afaf M. Babeer, M.I. Sayyed, H.Y. Morshidy, Abd El-razek Mahmoud, M.A. Abdo, M.S. Sadeq, High transparency of PbO–BaO–Fe_2O_3–SrO–B_2O_3 glasses with improved radiation shielding properties, Opt. Mater. 145 (2023) 114387.
[18] Jamila S. Alzahrani, S.N. Nazrin, Canel Eke, Imen Kebaili, M.S. Al-Buriahi, Aleesya Syaqira Joesry Syaiwan, Effect of strontium oxide on radiation shielding features and elastic properties on zinc borotellurite glass system, Radiat. Phys. Chem. 199 (2022) 110304.
[19] Abdullah Aloraini Dalal, Ashok Kumar, Aljawhara H. Almuqrin, M.I. Sayyed, Effect of adding SrO, TeO_2, PbO, and Bi_2O_3 heavy metal oxides on the optical and gamma ray shielding properties of Li_2O-K_2O-B_2O_3 glasses, Optik 247 (2021) 167848.
[20] Poussy Aly, A.A. El-Kheshen, Hanaa Abou-Gabal, Said Agamy, Structural investigation and measurement of the shielding effect of borosilicate glass containing PbO, SrO, and BaO against gamma irradiation, J. Phys. Chem. Solid. 145 (2020) 109521.
[21] Y. Al-Hadeethi, M.I. Sayyed, Manasa Nune, Radiation shielding study of WO_3–ZnO–PbO–B_2O_3 glasses using Geant4 and Phys-X: a comparative study, Ceram. Int. 47 (2021) 3988–3993.
[22] Erdem Şakar, Özgür Fırat Özpolat, Bünyamin Alım, M.I. Sayyed, Murat Kurudirek, Phy-X/PSD: development of a user-friendly online software for calculation of parameters relevant to radiation shielding and dosimetry, Radiat. Phys. Chem. 166 (2020) 108496.
[23] Gaurav Tyagi, Anupam Singhal, Srikanta Routroy, Dipendu Bhunia, Mukund Lahoti, A review on sustainable utilization of industrial wastes in radiation shielding concrete, Mater. Today: Proc. 32 (2020) 746–751.
[24] Hualiang Liu, Jianjun Shi, Huiqiong Qu, Dexin Ding, An investigation on physical, mechanical, leaching and radiation shielding behaviors of barite concrete containing recycled cathode ray tube funnel glass aggregate, Construct. Build. Mater. 201 (2019) 818–827.
[25] Nastasia Saca, Lidia Radu, Viorel Fugaru, Maria Gheorghe, Ionela Petre, Composite materials with primary lead slag content: application in gamma radiation shielding and waste encapsulation fields, J. Clean. Prod. 179 (2018) 255–265.
[26] A. Zughbi, M.H. Kharita, A.M. Shehada, Determining optical and radiation characteristics of cathode ray tubes' glass to be reused as radiation shielding glass, Radiat. Phys. Chem. 136 (2017) 71–74.
[27] Dariush Souri, Zahra Esmaeili Tahan, A new method for the determination of optical band gap and the nature of optical transitions in semiconductors, Appl. Phys. B 119 (2015) 273–279.
[28] B.M. Alotaibi, M.I. Sayyed, Ashok Kumar, Mohammed Alotiby, K.A. Mahmoud, Haifa A. Al-Yousef, N.A.M. Alsaif, Y. Al-Hadeethi, Fabrication of TeO_2-doped

strontium borate glasses possessing optimum physical, structural, optical and gamma ray shielding properties, European Physical Journal Plus 136 (2021) 468.
[29] Aljawhara H. Almuqrin, M.I. Sayyed, S. Hashim, Ashok Kumar, Exploring the impact of PbO/CdO composition on the structural, optical, and gamma ray shielding properties of dense PbO–TeO_2–CdO glasses, Opt. Mater. 138 (2023) 113698.
[30] Jamelah S. Al-Otaibi, Aljawhara H. Almuqrin, M.I. Sayyed, Ashok Kumar, Multifaceted analysis of PbO–Bi_2O_3–ZnO–B_2O_3 glasses: unveiling structural, Optical, and gamma-ray shielding behaviour, J. Mater. Sci. Mater. Electron. 34 (2023) 1721, https://doi.org/10.1007/s10854-023-11166-3.
[31] S. Rada, T. Ristoiu, M. Rada, I. Coroiu, V. Maties, E. Culea, Towards modeling gadolinium–lead–borate glasses, Mater. Res. Bull. 45 (2010) 69–73.
[32] K. Kotkova, H. Ticha, L. Tichy, Raman studies and optical properties of some of $(PbO)_x(Bi_2O_3)_{0.2}(B_2O_3)_{0.8-x}$ glasses, J. Raman Spectrosc. 39 (2008) 1219–1226.
[33] J. Leciejewicz, Neutron-diffraction study of orthorhombic lead monoxide, Acta Crystallogr. 14 (1961) 66.
[34] D.M. Adams, D.C. Stevens, Single-crystal vibrational spectra of tetragonal and orthorhombic lead monoxide, J. C. S. Dalton (1977) 1096–1103, https://doi.org/10.1039/DT9770001096.
[35] S. Feller, G. Lodden, A. Riley, T. Edwards, J. Croskrey, A. Schue, D. Liss, D. Stentz, S. Blair, M. Kelley, G. Smith, S. Singleton, M. Affatigato, D. Holland, M.E. Smith, E. I. Kamitsos, C.P.E. Varsamis, E. Ioannou, A multispectroscopic structural study of lead silicate glasses over an extended range of compositions, J. Non-Cryst. Solids 356 (2010) 304–313, https://doi.org/10.1016/j.jnoncrysol.2009.12.003.
[36] Z.Y. Yao, D. Moncke, E.I. Kamitsos, P. Houizot, F. Cʹelariʹe, T. Rouxel, L. Wondraczek, Structure and mechanical properties of copper-lead and copperzinc borate glasses, J. Non-Cryst. Solids 435 (2016) 55–68, https://doi.org/10.1016/j.jnoncrysol.2015.12.005.
[37] G.D. Chryssikos, J.A. Kapoutsis, A.P. Patsis, E.I. Kamitsos, A classification of metaborate crystals based on Raman spectroscopy, Spectrochim. Acta 47 (1991) 1117–1126, https://doi.org/10.1016/0584-8539(91)80043-I.
[38] A. Rulmont, M. Almou, Vibrational spectra of metaborates with infinite chain structure: $LiBO_2$, Ca_2BO_4, SrB_2O_4, Spectrochim Acta A, Mol. Biomol. Spectrosc. 45A (1989) 603–610, https://doi.org/10.1016/0584-8539(89)80013-3.
[39] Al-B.F. A. Mohammed, G. Lakshminarayana, S.O. Baki, M.K. Halimah, I.V. Kityk, M.A. Mahdi, Structural, thermal, optical and dielectric studies of Dy^{3+}: B_2O_3–ZnO–PbO– Na_2O–CaO glasses for white LEDs application, Opt. Mater. 73 (2017) 686–694.
[40] E.I. Kamitsos, M.A. Karakassides, G.D. Chryssikos, Vibrational spectra of magnesium-sodium-borate glasses. 2. Raman and mid-infrared investigation of the network structure, J. Phys. Chem. A 91 (1987) 1073–1079.
[41] E.M.A. Hussein, Y.S. Rammah, Optical UV–visible, Raman spectroscopy, and gamma radiation shielding properties of borate glass systems; B_2O_3 + Na_2O + Al_2O_3/MgO/Li_2O, Opt. Quant. Electron. 56 (2024) 387.
[42] M.S. Dahiya, S. Khasa, A. Agarwal, Structural, optical and thermal properties of transition metal ions doped bismuth borate glasses, Phys. Chem. Glasses: Eur. J. Glass Sci. Technol. B 57 (2016) 45–52.
[43] T. Vassilev, I. Penkov, C. Tzvetkova, R. Pascova, Glass transition temperatures and structures of multicomponent borate glasses: influence of modifier cation field strengths, J. Non-Cryst. Solids 438 (2016) 1–6.
[44] S.H.A. Aziz, H. Ahmad, Z.A. Wahab, Z.A. Sulaiman, Z.A. Talib, A.H. Shaari, H. B. Senin, Ultrasonic and thermal properties of borate and phosphate glasses containing bismuth and lead, AIP Conf. Proc. 909 (2007) 197–209.